Microwave Heating of Poly(ethylene terephthalate) Bottle Preforms Used in the Thermoforming Process

Philippe Lebaudy,[1] Lionel Estel,[2] Alain Ledoux,[2]

[1]*Laboratoire de Matériaux Macromoléculaires, Unité Mixte de Recherche du Centre National de la Recherche Scientifique 6522, Institut National des Sciences Appliquées de Rouen, Place Emile Blondel, BP 08, 76131 Mont-Saint-Aignan Cedex, France*
[2]*Département Maîtrise des Risques Industriels et Impacts sur l'Environnement, Institut National des Sciences Appliquées de Rouen, Place Emile Blondel, BP 8, 76131 Mont-Saint-Aignan Cedex, France*

Received 12 January 2007; accepted 11 July 2007
DOI 10.1002/app.27763
Published online 19 February 2008 in Wiley InterScience (www.interscience.wiley.com).

ABSTRACT: Thermoforming (free blowing) of poly(ethylene terephthalate) preforms was successfully and quickly performed in a rotating system designed for dielectric hysteresis heating. Temperature profile modeling was carried out with the amorphous poly(ethylene terephthalate) permittivity at different temperatures. The Maxwell and heat equations were used to determine the best profile and power tuning. The determination of the theoretical boundary conditions was accomplished by the adjustment of the numerical transient external surface wall temperature with experimental infrared pyrometry results. In comparison with infrared, microwaves allowed high power density absorption inside the perform wall without a dramatic temperature gradient. Consequently, the heat blowing stage could be accelerated, and the process took at least 5 times less energy than infrared heating. Industrial applications involve the integration of the molding step and the design of the overall process. © 2008 Wiley Periodicals, Inc. J Appl Polym Sci 108: 2408–2414, 2008

Key words: irradiation; modeling; polyethylene (PE)

INTRODUCTION

Injection blow molding is in use for the production of hollow objects in large quantities. This technology is mainly applied to the manufacture of poly(ethylene terephthalate) (PET) bottles, jars, and other containers. The injection blow molding process produces bottles of superior visual and dimensional quality in comparison with extrusion blow molding. This process is a two-step process, and two molds are required. In the first step, a mandrel is placed in the first mold, and the thermoplastic material is then injected into the mold flowing around the mandrel to create a preform. After cooling, the preforms are usually stocked a couple of days. In the second step, the PET preform must be brought to a rubberlike state by heat before its transfer to a second mold to be blown with compressed air and to expand to the shape of the mold. During this step, the material is biaxially oriented to produce stronger products. For this second process, the heating stage is critical for the following reasons.

First, the final thickness distribution of the part is drastically controlled by the temperature distribution inside the preform before its formation. Furthermore, when solid and amorphous PET is biaxially oriented, the stretching action and the temperature at which it occurs determine the level of crystallinity of the final product.[1] In biaxial-stretch blow molding of bottles, the outer and inner stretching ratios differ by more than 50% during stretching (inner stretching ratio = 4, outer stretching ratio = 6.5). On the basis of the mechanical behavior of amorphous PET at different temperatures,[1] it appears that for a given temperature, the actual stress is higher inside the wall than outside the wall. As uniformity of stress is required, a good stretching process is obtained by deliberate induction of a nonuniform temperature profile throughout the preform before blowing.

A second reason is the thermal crystallization ability of the material, which is again critical for the heating stage. Once the polymer goes through the crystallization temperature (T_c) range (110–140°C), the resulting crystalline fraction is characterized by a spherulitic morphology, in which the resulting cooled part will be opaque. Moreover, a high crystalline fraction makes stretch blow molding impossible. Therefore, the temperature inside the wall of the part must be in the range of 80 [the glass-transition temperature (T_g) to 110°C (T_c).

In previous works,[1–3] it has been shown that heating by an infrared oven with an infrared emitter

Correspondence to: P. Lebaudy (philippe.lebaudy@insa-rouen.fr.).

Contract grant sponsor: Scientific Council of the Institut National des Sciences Appliquées de Rouen.

combined with strong surface cooling allows both a nonuniform profile temperature and a temperature range of T_g–T_c to be obtained. This method ensures a good stretching process, which is convenient and widely used in the industrial process.

The usual mechanisms of heat transfer by infrared radiation are explained in these previous studies and are outside the scope of this work.[3] It is sufficient to note that the Lambert–Bouguer law is used to describe the spectral absorption characteristics of the materials. Unfortunately, although many studies have been devoted to optimizing this process,[1–5] in most industrial infrared ovens, the ratio of the electric power to the absorbed energy in the polymer is less than 20%, and the heating time is still high (25 s).

The aim of this article is to demonstrate the technical feasibility of the free blowing of bottles preforms with microwaves as a heat source. Today, microwaves are effectively a technology that brings improvements to the performance of complex devices together with a reduction in the size and cost of production. In research and industrial applications, microwaves are used principally in telecommunications and materials processing. In recent years, rapid development in microwave equipment and the modification of ovens has been witnessed. Marked growth in the field of microwave technology development is evident from the number of publications and patents.[4–12] Since the early 1960s until today, there has been a great deal of interest in microwave processing of polymeric materials worldwide.[13] At present, if dielectric heating is widely employed industrially for thermoforming of plastics, few examples exist in the preheating of plastics before molding.

THEORETICAL

Microwave dielectric heating characteristics

Energy conversion

The electromagnetic interaction of a material depends on the dielectric loss permittivity of the material. The real part, called the relative dielectric constant (ε_r'), defines the ability of a material to be polarized under an electromagnetic field. The complex part, called the relative dielectric loss (ε_r''), defines the effectiveness of a material in converting electromagnetic energy into heat. As a result of the dielectric loss and penetration depth within materials, microwave absorption provides a volumetrically distributed heat source. The complex dielectric permittivity is dependent on the frequency, temperature, and material nature.[14] In eq. (1), tan δ defines the ability of a material with ε_r'' to convert electromagnetic energy into thermal energy at a fixed temperature and frequency:

$$\tan \delta = \frac{\varepsilon_r''}{\varepsilon_r'} \tag{1}$$

The dissipated microwave irradiation power density inside materials at any radial position r [$P(r)$] is given by eq. (2):

$$P(r) = \pi \cdot f \cdot \varepsilon_0 \cdot \varepsilon_r''(r) \cdot (E(r) \cdot E^*(r)) \tag{2}$$

where f is the excitation frequency; $E(r)$ and $E^*(r)$ are the local electric field intensity and its conjugate, respectively; and ε_0 is the free space permittivity (F/m). The dielectric constant and loss determine the wavelength (λ) and the penetration depth (D_p) within materials as follows:

$$\lambda = \frac{\lambda_0}{\sqrt{\frac{\varepsilon_r'}{2}\left(\sqrt{1 + (\tan \delta)^2} + 1\right)}} \tag{3}$$

$$D_p = \frac{\lambda_0}{\pi\sqrt{2\varepsilon_r'\left(\sqrt{1 + (\tan \delta)^2} - 1\right)}} \tag{4}$$

where λ_0 corresponds to the wavelength in free space (in air, λ_0 = 12.24 cm for f = 2.45 GHz).

Measurements of the dielectric properties

As described in a previous article,[15] dielectric measurements were carried out with the small perturbation of a resonant cavity method. In this method, the perturbations caused by a sample to the frequency and amplitude of the cavity electromagnetic resonance are compared to standards to determine its complex permittivity. Dielectric properties of PET are a function of the temperature. As shown in Figure 1, the real and imaginary parts slowly increase from the ambient temperature to T_g.

As a result, PET stores more electromagnetic energy as the temperature increases, with no specific influence of crystallization. This energy will not be converted into heat more efficiently before T_g, but this conversion will increase after T_g. The loss tangent, defined by the ratio of the imaginary and real parts of the permittivity, characterizes this behavior. The ratio slowly increases from 7×10^{-3} to 1.2×10^{-2} between 40 and 80°C and is still rising between 80 and 120°C, reaching 2.6×10^{-2}.

Experimental apparatus and procedures

According to Figure 2, the microwave heating system consisted of a magnetron working at 2.45 GHz with a maximal nominal power of 1950 W. Microwaves were carried in a WR 340 waveguide applica-

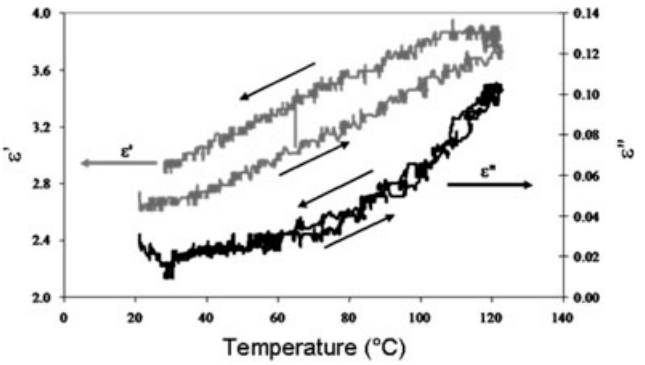

Figure 1 Measurement of the complex dielectric permittivity properties of PET versus the temperature. The real part is the relative dielectric constant (ε′), and the complex part is the relative dielectric loss (ε″).

tor (Microondes Energie Systemes Technologies, France) for resonant single-mode transverse electric mode 103 (TE_{103}) propagation. Cylindrical samples were introduced through a tube small enough to prevent microwave leakage. A short circuit was used to keep the reflected power to a minimum. The circulator protected the magnetron by diverting the reflected power into a water load. This system was also equipped with probes to measure the reflected and the incident powers.

A PET preform (AKZO D04-300 IV 0.85, Nestlé (France); height = 5.6 cm, external diameter = 1.7 cm, internal diameter = 0.9 cm) was placed in the cavity screwed onto the end of a polytetrafluoroethylene handler. This polytetrafluoroethylene handler was connected to a varying-speed rotating system. The temperature of the sample surface was measured through a side window with a Minolta/Land Cyclops 300AF infrared pyrometer (Minolta, France). The preform consisted of a full bottle neck with a thick tube of polymer attached, which formed the body.

Numerical simulation and results

Electromagnetic simulation results

Theoretical considerations. A propagating electromagnetic wave is composed of oscillating electric (E) and magnetic (H) field components. Maxwell's equations, describing their space and time dependence, are as follows:

$$\nabla \times E = -\frac{\partial B}{\partial t} \tag{5}$$

$$\nabla \times H = J + \frac{\partial D}{\partial t} \tag{6}$$

where B is the magnetic induction (Wb/m^2), J is the current density (A/m^2) D is the electric displacement (C/m^2), and t is the time (t). Alternately, one may recast the source-free forms of Maxwell's equations in the frequency domain to obtain the Helmholtz equations:

$$\nabla^2 E - \gamma^2 E = 0 \tag{7}$$

$$\nabla^2 H - \gamma^2 H = 0 \tag{8}$$

where $\gamma = \alpha + j\beta$ is the longitudinal propagation constant (1/m). α is the phase factor (1/m), j is a pure imaginary number, and β is the attenuation factor (1/m):

$$\gamma^2 = -\omega^2\mu\varepsilon + j\omega\mu\sigma \tag{9}$$

where μ is the magnetic permeability (H/m), ε is the permittivity (F/M), σ is the electric conductivity ($1/\Omega$ m), and ω is the angular frequency (rad/s). In this heating application, magnetic effects are negligible; $\mu(\omega)$ is well approximated by its value in free space (μ_0). Because the timescale of electromagnetic propagation is significantly lower then the timescales for thermal diffusion, the time derivatives of $\sigma(\omega)$ and $\varepsilon(\omega)$ are very low and have been ignored. Therefore, a solution with all the possible resonant modes in Cartesian coordinates takes into account all the components of electric and magnetic fields [$E(x,y,z)$ and $H(x,y,z)$, respectively]. With the longitudinal components E_y and H_y denoted Ψ, for propagation in the x direction in the waveguide, we obtain the following propagation equation:

$$\Delta\Psi + \mu\varepsilon\omega^2\Psi = 0 \tag{10}$$

Because every possible solution to governing equations of propagation in a waveguide can be decomposed into the linear combination of TE and transverse magnetic mode expressions (see refs. 16 and 17 for a more refined discussion), the contribution of transverse electric mode and TM modes must be considered.

Solving field equations. In this study, field equations were solved on a two-dimensional representative

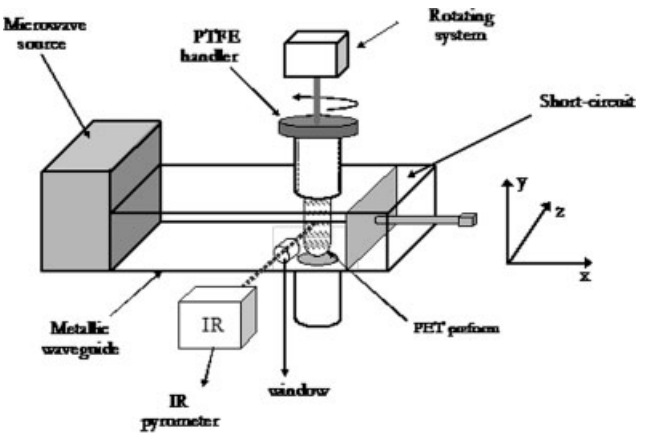

Figure 2 Experimental apparatus. The short circuit is used to adjust the cavity and keep the reflected power to a minimum.

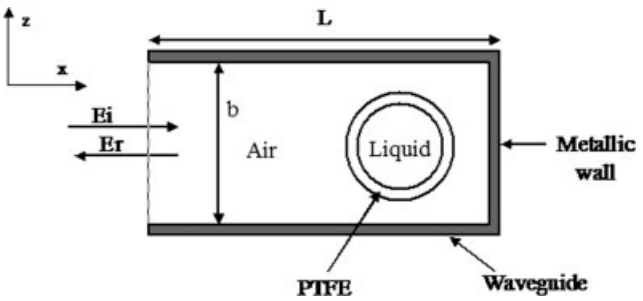

Figure 3 Geometry for numerical evaluations: cross-sectional view of the waveguide.

geometry, as shown in Figure 3. It corresponds to a transversal cross section of the waveguide and the reactor. No analytical solution of differential equations in such a complex geometry is possible. A numerical approach is necessary. Solutions are obtained by a finite element method. Assuming the electrical field to have only one component perpendicular to the considered section, the equation of propagation can be written as follows:

$$\frac{\partial^2 E_{y,m}}{\partial x^2} + \frac{\partial^2 E_{y,m}}{\partial z^2} + k_{pm}^2 E_{y,m} = 0 \tag{11}$$

where subscript m represents any geometrical area (air, PET, or metallic wall) and k_p is the propagation constant (1/m).

In the waveguide, three of the four sides are well defined because they materialize as a metallic wall. The Dirichlet condition can then be used [eq. (6)]:

$$\left.\begin{aligned} E_y(x,0) &= 0 \\ E_y(x,b) &= 0 \end{aligned}\right\} \quad 0 < x < L$$
$$E_y(L,z) = 0 \qquad 0 < z < b \tag{12}$$

where b is the waveguide height (m) and L the wave guide length (m). The fourth side is the entrance of the waveguide. The resulting field is a superposition of an incident field coming from the left and a reflected field coming from the right along the x axis. If E_0 is the intensity of the source, the reflected field has a lower intensity defined by RE_0, where R is the reflection coefficient. The resultant field can be written as follows:

$$E_y(x,z) = E_0 \exp(-jk_p x) + RE_0 \exp(jk_p x) \tag{13}$$

In the present state, eq. (7) cannot be used in the mathematical model. Taking the derivative of this equation and considering that boundary is at $x = 0$, we get

$$\frac{dE_y}{dx} - jk_p E_y = -2jk_p \tag{14}$$

Finally, the interface conditions on the reactor between air and PET are obtained by the conservation of the tangential component of the electrical field.

In this study, simulations were started with average constant dielectric properties (relative permittivity (ε_r) = 3.0–0.06j). We can observe in Figure 4 that dissipated power exists on all the sections of the preform. Along the radius, this power increases slightly from the external face to the internal face. This temperature profile is in good agreement with the temperature constraint introduced by the free blow. The evolution of the permittivity will probably emphasize this particular energy distribution. Microwave heating leads to an operational temperature distribution; that is, there is no need for a heating/cooling cycle like infrared heating.

Temperature profile simulation

Theoretical considerations. No flow or molecular diffusion is developing inside the preform wall, so heat is transferred only by conduction. Numerical calculations are based on the heat diffusion equation in cylindrical coordinates with one location-dependent heat source:[20]

$$\rho c_p \frac{\partial T}{\partial t} = \frac{\partial}{\partial z}\left(k\frac{\partial T}{\partial z}\right) + \frac{1}{r}\frac{\partial}{\partial r}\left(kr\frac{\partial T}{\partial r}\right) + \frac{1}{r^2}\frac{\partial}{\partial \theta}\left(k\frac{\partial T}{\partial \theta}\right) + S(r) \tag{15}$$

where T is the temperature (°C), t is the time (s), r is the radial position (m), $S(r)$ is the location-dependent heat source that corresponds to the microwave power density inside the preform (Fig. 4), k (W/m K) is the thermal conductivity, c_p is the specific heat capacity (J/kg K), and ρ is the density (kg/m^3). All

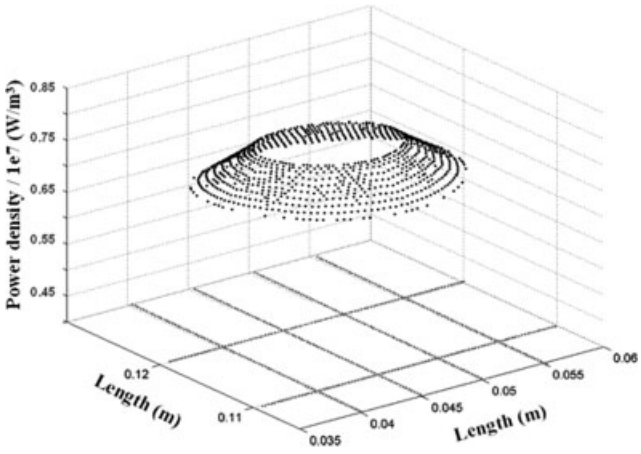

Figure 4 Microwave power density calculation inside the PET preform [$S(r)$].

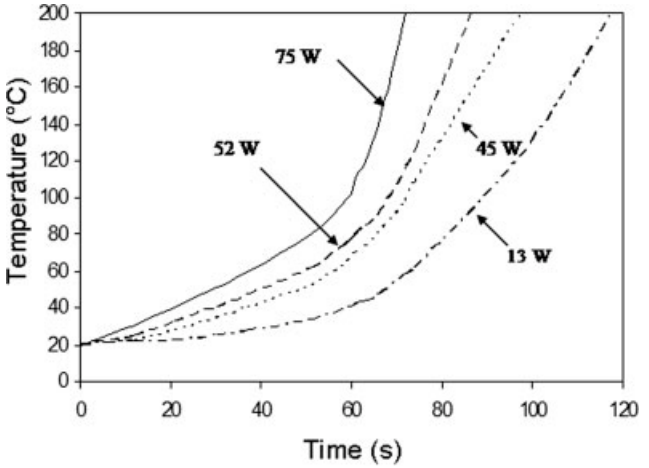

Figure 5 Adjustment of the resonant cavity at $P = 200$ W.

thermal parameters such as k and c_p are assumed to be constant during the entire experiment. In this form, because of the location-dependent heat source generated by the microwave absorption, eq. (15) has no obvious analytical solution and cannot be integrated mathematically. The problem was solved with an explicit numerical method with finite differences.[19]

Initial and boundary conditions. Initially ($t = 0$), the temperature throughout the sample is assumed to have a uniform value (T^0). At time t, the flux across the external surface is proportional to the difference between the surface temperature (T_S^t) and the air temperature (T_{air}), and the internal surface is assumed to be adiabatic:

$$\left.\frac{\partial T^t}{\partial r}\right|_{r=R_e} = -\frac{h}{k}(T_s^t - T_{\text{air}}) \tag{16}$$

$$\left.\frac{\partial T^t}{\partial r}\right|_{r=R_i} = 0 \tag{17}$$

where R_e and R_i are external and internal radius of the preform, and $h = 10$ W/m^2 K is the average heat convective coefficient. We approximated this coefficient by taking into account the heat-transfer correlation [eq. (18)] for a rotating cylinder[19] and the free convection on a vertical wall correlation[18] [eq. (19)]:

$$\overline{Nu} = 0.6366\,(RePr)^{1/2} \tag{18}$$

$$\overline{Nu}_L = \left\{0.825 + \frac{0.387\,Ra_L^{1/6}}{\left[1 + (0.492/Pr)^{9/16}\right]^{8/27}}\right\}^2 \tag{19}$$

where Re, Pr, Ra, and Nu are the dimensionless numbers of Reynolds (rotating), Prandtl, Rayleigh, and Nusselt.

RESULTS AND DISCUSSION

As previously described, a PET preform at room temperature is placed in the chimney for all the following measurements. In a first step, the dielectric heating is optimized by the tuning of the cavity thanks to the short circuit (see Fig. 2). Indeed, at a constant input power of 200 W, the temperature behavior is tuning-dependent, as shown in Figure 5. The four curves correspond to different moving short-circuit positions leading to different absorbed powers (the absorbed power values correspond to the initial values during the experiment). The better the tuning is, the more rapid the heating is. The slope break around T_g can be explained by a change in the material permittivity with the temperature according to the results in Figure 1. An increase in the loss tangent implies a better energy conversion of electromagnetic energy into heat, influencing the dissipated power density.

In a second step, with the optimum tuning, different input powers are applied up to 500 W. For high input powers and as expected, the temperature of blowing is obtained with a short delay (Fig. 6). This figure can be broken down into two parts. In the first part, when the temperature is below T_g, the preform temperature increases linearly and gently with time. This can be explained by the fact that the material dielectric permittivity increases linearly with the temperature (Fig. 1). In the second part of the figure, that is, from T_g to T_c, the preform temperature raises sharply. This sharp rise is due to the significant increase of the dielectric permittivity value after T_g.

The numerical calculation gives the transient surface temperature and the temperature profile inside the PET wall. Unfortunately, only the external surface temperature is experimentally measurable with an infrared pyrometer. Consequently, validation of

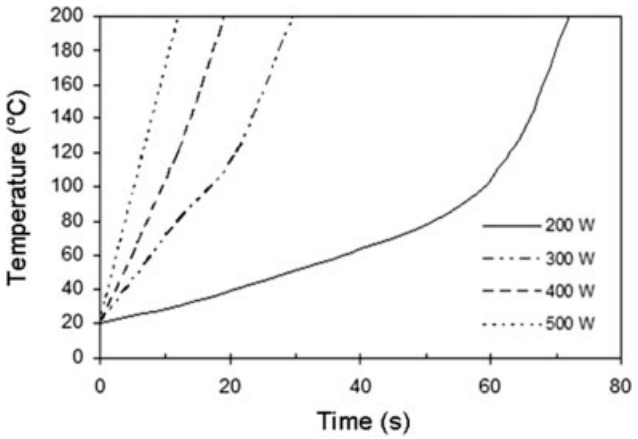

Figure 6 Temperature profile evolution inside the PET wall for microwave power densities of 200, 300, 400, and 500 W after optimization of the cavity.

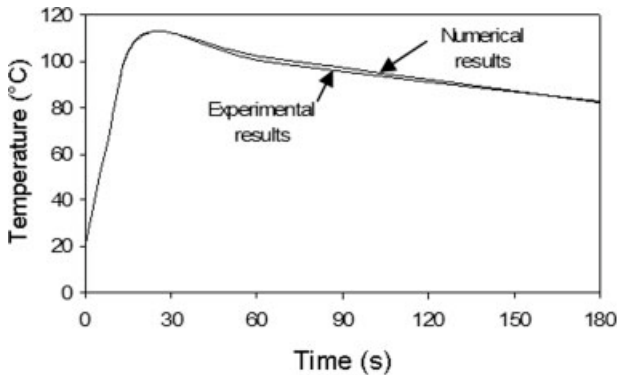

Figure 7 Comparison of the numerical and experimental external surface transient temperatures.

the numerical calculation can be done only by comparison of the experimental and theoretical surface temperature evolution. Moreover, this comparison allows the adjustment of the theoretical boundary condition parameter to obtain good temperature concordance (Fig. 7).

We can now observe in Figure 8 the simulated temperature profile inside the PET wall just after the end of heating. The curve shows that the temperature profile obtained by this microwave process limits the inhomogeneity of stress and allows good stretch blow molding. The following profile is reached after a 20-s heating time with a 300-W microwave input power.

As previously mentioned, the heating time to obtain the temperature range of blowing (T_g–T_c) decreases when the microwave power increases, and for high microwave power inputs (>400 W), the temperature rises in a few seconds from T_g to T_c. The global trend of the curve is asymptotic. The temperature is obtained by infrared surface emission. Some delay, depending on the thermal transfer characteristic time, is necessary to observe a temperature change when microwave heating is on. This delay

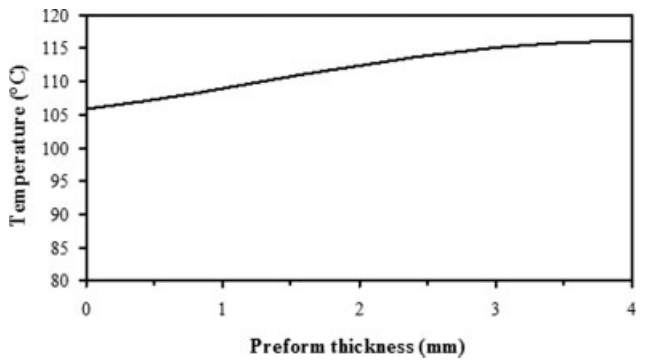

Figure 8 Simulated temperature profiles inside the PET wall.

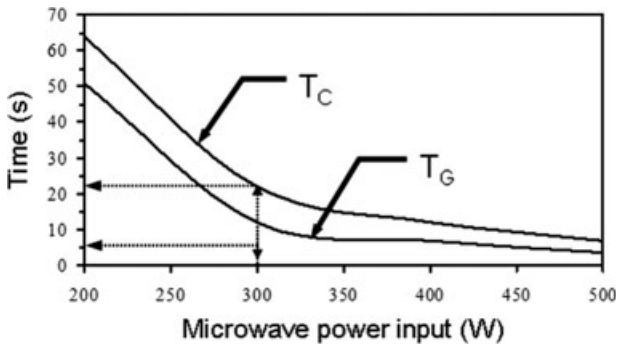

Figure 9 Heating time versus the microwave power input.

explains the incompressible time for high-power irradiation. Our different experiments concerning the heating time versus the microwave power input are summarized in Figure 9. We can see as an example that for a 200-W microwave power input, T_g is obtained in 50 s and T_c is obtained in 65 s. For nearly 15 s, the PET temperature allows good blowing of the preform. On the other hand, a 500-W microwave power input allows only 3 s at the blowing temperature, and it is going to be impossible to manually perform the process. For this last reason, high-power inputs have not been investigated in this study. Nevertheless, according to the temperature profile obtained by a 400-W microwave power input, it seems to be possible with electronic regulation to increase the microwave power up to 1000 W.

CONCLUSIONS

Partial free blowing of PET preforms has been successful, and our first results indicate that this technique has great potential for the preform heating stage. In comparison with infrared, microwaves allow high power density absorption inside the preform wall without the creation of an unadapted temperature gradient. Moreover, microwave power distribution inside a PET preform is appropriate for the nonuniform temperature profile expected throughout the preform wall before blowing, and consequently, it is not necessary to apply strong surface cooling. This last point is favorable for a better overall process efficiency and a lower process time. Indeed, because of the high available microwave power density together with the overall automation of the final industrial process, the heat blowing stage can be accelerated up to 5 times. At the moment, a standard waveguide applicator has been used; further research is needed to optimize the electromagnetic field and object interaction to produce lower reflected power and consequently a better energy yield.

NOMENCLATURE

Symbols

b	waveguide height (m)
B	magnetic induction (Wb/m^2)
c_p	specific heat capacity (J/kg K)
D	electric displacement (C/m^2)
D_p	penetration depth (m)
E	electric field (V/m)
$E(r)$	local electric field intensity (V/m)
$E^*(r)$	conjugate of the local electric field intensity (V/m)
f	excitation frequency (Hz)
h	heat-transfer coefficient (W/m^2 K)
H	magnetic field intensity (A/m)
j	pure imaginary number
k	thermal conductivity (W/m K)
k_p	propagation constant (1/m)
Nu	Nusselt number (—)
P	microwave source term (W/m^3)
Pr	Prandtl number (—)
r	radial position (m)
R	reflection coefficient (—)
Ra	Rayleigh number (—)
Re	Reynolds number (—)
S	microwave source term (W/m^3)
t	time (s)
T	temperature (K)
T_{air}	air temperature (°C)
T_c	crystallization temperature (°C)
T_g	glass-transition temperature (°C)
T_S^t	surface temperature (°C)

Greek letters

α	phase factor (1/m)
β	attenuation factor (1/m)
γ	longitudinal propagation constant (1/m)
δ	loss angle (rad)
ε	permittivity (F/m)
ε'	relative dielectric constant (—)
ε''	relative dielectric loss (—)
ε_0	free space permittivity (F/m)
ε_r'	relative dielectric constant (—)
ε_r''	relative dielectric loss (—)
λ	wavelength (m)
λ_0	wavelength in free space (m)
μ	permeability (H/m)
μ_0	free space permeability (H/m)
ρ	density (kg/m^3)
σ	electric conductivity (1/Ω m)
Ψ	longitudinal components E_z and H_z
ω	angular frequency (rad/s)

Subscripts and superscripts

0	source
m	geometrical area
r	relative property
t	time

References

1. Lebaudy, P.; Grenet, J. J Appl Polym Sci 2001, 80, 2683.
2. Lebaudy, P.; Saiter, J. M.; Grenet, J.; Vautier, C. Polymer 1992, 33, 1887.
3. Lebaudy, P.; Saiter, J. M.; Grenet, J.; Vautier, C. Polymer 1995, 36, 1217.
4. Schmidt, F. M.; Le Maoult, Y.; Monteix, S. J Mater Process Technol 2003, 143, 225.
5. Hasna, A. M. J Mater Prod Technol 2003, 19, 259.
6. Data, K.; Anantheswaran, R. C. Handbook of Microwave Technology for Food Applications; Data, K.; Anantheswaran, R. C., Eds.; 2001.
7. Mudgett, R. E. In Biotechnology and Food Process Engineering; Schwartzberg, H. G.; Rao, A. M., Eds.; Marcel Dekker: New York, 1990; p 350.
8. Van Loock, W. M. I. V. Ceram Trans 1997, 80, 619.
9. Loupy, A., Ed.; Microwaves in Organic Synthesis; Wiley-VCH: Weinheim, 2002.
10. Zong, L.; Zhou, S.; Sgriccia, N.; Hawley, M. C.; Kempel, L. C. J Microwave Power Electromagn Energy 2003, 38, 49.
11. Yarlagadda Prasad, K. D. V.; Chuan, C. T. J Mater Process Technol 1998, 74, 199.
12. Hernández, M. T.; González, M. J Eur Ceram Soc 2002, 22, 2861.
13. Lester, E.; Kingman, S.; Wong, K. H.; Rudd, C.; Pickering, S.; Hilal, N. J Mater Res Bull 2004, 39, 1549.
14. Metaxas, C.; Meredith, R. J. In Industrial Microwave Heating; Perigrinus, P., Ed.; CheRD Part A, Elsevier: London, 1983.
15. Estel, L.; Bonnet, C.; Delmotte, M.; Cosmao, J. M. Chem Eng Res Des A 2003, 81, 1212.
16. Stratton, J. A. Electromagnetic Theory; McGraw-Hill: New York, 1941.
17. Gouesbet, G.; Gréhan, G. Atomization Sprays 2000, 10, 277.
18. Lienhard, I. V. J. H.; Lienhard, V. J. H. A Heat Transfer Textbook, 3rd ed.; Phlogiston: Cambridge, MA, 2002.
19. Carslaw, H. S.; Jaeger, J. C. Conduction of Heat in Solids, 2nd ed.; Clarendon: Oxford, 1959.
20. De Vriendt, A. B. In Transmission de la Chaleur; Morin, G., Ed.; Chicoutimi: Québéc, 1987; p 1.